Loperamide enhances the radiosensitivity of cervical cancer cells via ferroptosis induction

HUARONG GUO[1*], HAIXIA LI[1*], SHUNKANG TIAN[1], YUNKAI ZHANG[1], FUYUN WU[1,2] and JING KE[1,3]

[1]School of Basic Medical Sciences, Hubei University of Medicine, Shiyan, Hubei 442000, P.R. China; [2]Institute of Geriatric Medicine, Sinopharm Dongfeng General Hospital, Hubei University of Medicine, Shiyan, Hubei 442000, P.R. China; [3]Hubei Regional Medical Center for Geriatric Disease, Sinopharm Dongfeng General Hospital, Hubei University of Medicine, Shiyan, Hubei 442000, P.R. China

Received April 10, 2026; Accepted September 14, 2026

DOI: 10.3892/or.2026.9203

Abstract. Cervical cancer is a malignant tumor that threatens women's health and radiotherapy represents a major therapeutic approach for its treatment; however, radioresistance frequently leads to treatment failure. The present study aimed to investigate whether loperamide (LOP), a μ-opioid receptor agonist commonly used as an antidiarrheal agent, could enhance the radiosensitivity of cervical cancer cells by regulating ferroptosis. A Cell Counting Kit-8 assay was used to evaluate the cytotoxicity of LOP in SiHa and HeLa cells, and EdU and colony formation assays were performed to assess cell proliferation. In addition, wound-healing and Transwell assays were performed to detect cell migration. Flow cytometry was applied to measure cell apoptosis and intracellular reactive oxygen species (ROS) levels, and colorimetric assays were used to determine malondialdehyde (MDA) and glutathione (GSH) contents. The mRNA and protein expression levels of the ferroptosis-related markers GSH peroxidase 4 (GPX4) and solute carrier family 7 member 11 (SLC7A11) were analyzed using reverse transcription-quantitative PCR and western blotting. The results showed that LOP significantly inhibited the viability of SiHa and HeLa cells, and exerted a synergistic effect with radiotherapy (combination index <1) to suppress cell proliferation and migration. Combined treatment with LOP and radiotherapy markedly increased apoptosis and ROS accumulation, elevated MDA levels and reduced GSH levels. Moreover, the combination treatment significantly downregulated the expression of GPX4 and SLC7A11. These findings indicated that LOP enhances the radiosensitivity of cervical cancer cells, with ferroptosis induction via inhibition of the GPX4/SLC7A11 axis as a contributing mechanism. Both apoptosis and ferroptosis were induced by the combination treatment, suggesting that the radiosensitizing effect may involve multiple cell death pathways. These observations provide a basis for further investigation into LOP as a potential radiosensitizing agent in cervical cancer.

Correspondence to: Professor Fuyun Wu or Ms. Jing Ke, School of Basic Medical Sciences, Hubei University of Medicine, 30 South Renmin Road, Maojian, Shiyan, Hubei 442000, P.R. China
E-mail: wufuyun@hbmu.edu.cn
E-mail: kejingjing@hbmu.edu.cn

*Contributed equally

Key words: loperamide, ferroptosis, radiosensitization, cervical cancer

Introduction

Cervical cancer is the fourth most common malignancy in women worldwide, with disproportionately high incidence and mortality rates in developing countries. In 2022, an estimated 662,044 new cases of cervical cancer and 348,709 associated deaths occurred globally, with the majority reported in low- and middle-income countries (1). Treatment strategies are stratified by stage, with radiotherapy serving as a common treatment option, either as a definitive modality or adjuvant therapy (2-4). Despite advances in radiation techniques, treatment outcomes are frequently compromised by the development of intrinsic or acquired radioresistance, which contributes to locoregional recurrence and poor prognosis. The mechanisms driving radioresistance are complex and multifaceted, encompassing enhanced DNA repair capacity, dysregulated cell cycle checkpoints, hypoxia-induced survival signaling and evasion of programmed cell death. Among these, resistance to radiation-induced apoptosis has been extensively investigated; however, therapeutic interventions designed to restore apoptotic sensitivity have achieved only limited clinical success (5,6). This therapeutic bottleneck has prompted growing interest in alternative forms of regulated cell death that may bypass apoptotic resistance pathways (7-10).

Ferroptosis is a relatively recently identified form of regulated cell death driven by iron-dependent lipid peroxidation, which has garnered notable attention in oncology. This non-apoptotic pathway is defined by the excessive accumulation of lipid reactive oxygen species (ROS), which surpasses the scavenging capacity of glutathione (GSH) peroxidase 4 (GPX4), ultimately leading to membrane lipid rupture and cell death (11,12). Notably, ionizing radiation not only generates ROS directly through water radiolysis but also facilitates lipid peroxidation by producing hydroxyl radicals that attack polyunsaturated fatty acids within cellular membranes. Under

physiological conditions, the solute carrier family 7 member 11 (SLC7A11)/GPX4 antioxidant axis effectively counteracts this oxidative challenge by reducing lipid hydroperoxides to non-toxic lipid alcohols. However, when this protective system is functionally compromised, either by overwhelming oxidative stress or pharmacological inhibition, cells become highly susceptible to ferroptotic death. Emerging evidence has established a mechanistic link between ferroptosis defense and radiation resistance. Notably, radioresistant cancer cells frequently exhibit upregulated expression of SLC7A11 and GPX4, suggesting that reinforced ferroptosis protection is an adaptive survival mechanism against radiotherapy-induced oxidative injury (13-15). Conversely, pharmacological induction of ferroptosis has been shown to effectively sensitize various tumor types to ionizing radiation, including glioma, colorectal cancer, triple-negative breast cancer and non-small cell lung cancer (16-19). Given that radiotherapy itself generates ROS, potential crosstalk between ferroptosis and radiation response is biologically plausible. Consistent with this, targeting ferroptosis has emerged as a promising strategy to promote the radiosensitivity of cancer cells (20,21). However, the relative contribution of ferroptosis versus other forms of cell death to radiation sensitization remains context-dependent and requires further investigation.

Loperamide (LOP), a μ-opioid receptor agonist, is a long-acting antidiarrheal agent clinically used for the management of acute and chronic diarrhea of various etiologies, and is commonly employed for the symptomatic treatment of radiation enteritis or radiotherapy-associated diarrhea (22,23). Previous studies have demonstrated that LOP also inhibits the viability and proliferation of tumor cells by inducing autophagy and suppressing the expression of multidrug resistance 1, exhibiting promising therapeutic efficacy in glioblastoma, breast cancer and other malignancies (24,25). In addition, LOP has been reported to interact with the efflux transporter P-glycoprotein, which is commonly upregulated in radioresistant tumors and contributes to treatment failure (26). These observations indicate that LOP may exert pleiotropic effects on cancer cells beyond its original indication. However, to the best of our knowledge, whether LOP can modulate ferroptosis and influence the radiosensitivity of cervical cancer cells remains unexplored. Given that radiotherapy promotes oxidative stress and ferroptosis is driven by iron-dependent lipid peroxidation, it was hypothesized that LOP may disturb cellular redox homeostasis and act in combination with irradiation to promote ferroptotic cell death, thereby contributing to enhanced radiosensitivity.

Therefore, the present study aimed to investigate whether LOP perturbs the cellular redox balance and triggers ferroptosis in cervical cancer cells, thereby enhancing their radiosensitivity. Elucidating this mechanism may provide a basis for repurposing LOP as a potential radiosensitizing agent in cervical cancer therapy.

Materials and methods

Cell culture. Human cervical cancer HeLa cells and human cervical squamous cell carcinoma SiHa cells were purchased from Procell Life Science & Technology Co., Ltd. All cell lines were authenticated using short tandem repeat profiling and were verified to be free of mycoplasma contamination before use in the present study. Cells were routinely cultured in DMEM (cat. no. 11995065; Gibco; Thermo Fisher Scientific, Inc.) supplemented with 10% (v/v) fetal bovine serum (FBS; cat. no. 10099141; Gibco; Thermo Fisher Scientific, Inc.) and a penicillin-streptomycin mixture (100 U/ml and 100 μg/ml, respectively) in a humidified incubator maintained at 37˚C with 5% CO_2.

X-ray irradiation. X-ray irradiation was performed using an X-RAD 320 irradiator (Precision X-Ray, Inc.), with a source-to-surface distance of 50 cm and a field size of 20x20 cm^2, at a dose rate of 2.0 Gy/min. The irradiation duration was 1 min for 2 Gy, 2 min for 4 Gy, 3 min for 6 Gy, 4 min for 8 Gy and 5 min for 10 Gy. All irradiations were performed at room temperature and the culture plates were positioned to ensure uniform dose delivery across the entire well surface. For all experiments, cells were divided into four groups: i) DMSO control group, in which cells were treated with an equal volume of DMSO as that used to dissolve LOP in the LOP and R + LOP groups (final concentration <0.1%, v/v) for 48 h at 37˚C; ii) R group, in which cells were exposed to 6 Gy X-ray irradiation alone (dose rate, 2.0 Gy/min; exposure duration, 3 min) at room temperature; iii) LOP group, in which cells were treated with 15 μM LOP (cat. no. HY-B0418A; MedChemExpress) alone for 48 h at 37˚C; and iv) R + LOP group, in which cells were treated with 15 μM LOP for 4 h at 37˚C prior to exposure to 6 Gy X-ray irradiation (dose rate, 2.0 Gy/min; exposure duration, 3 min) and maintained in the presence of the drug throughout the remainder of each experiment. Unless otherwise indicated, cells were cultured for a total of 48 h before analysis.

Cell Counting Kit-8 (CCK-8) assay. Cells were counted and seeded into 96-well microplates at a density of 3,000 cells/well. On the following day, two sets of experiments were performed. For the LOP cytotoxicity assay, cells were treated with LOP alone for 48 h at 37˚C without irradiation; the concentrations used were 0, 5, 10, 20, 40 and 80 μM for SiHa cells, and 0, 10, 20, 40, 80 and 160 μM for HeLa cells. For the combination experiments, cells were treated with LOP at 0, 5, 10, 20, 40 and 80 μM for 4 h at 37˚C, followed by X-ray irradiation at 0, 2, 4, 6 8 and 10 Gy (dose rate, 2.0 Gy/min; exposure duration, 1, 2, 3, 4 and 5 min, respectively). LOP was dissolved in DMSO with a final concentration of <0.1% (v/v), which had no notable effect on cell viability. After 48 h of culture, the culture medium was removed, and 100 μl fresh DMEM containing 10 μl CCK-8 solution was added to each well, followed by an additional 2 h incubation at 37˚C. The optical density value at 450 nm was determined using a multifunctional microplate reader (SpectraMax 190; Molecular Devices, LLC). The half-maximal inhibitory concentration (IC_{50}) was calculated accordingly. The combination index (CI) was calculated using CompuSyn software (version 1.0; ComboSyn, Inc.) based on the Chou-Talalay method (27). The fraction affected (Fa) represents the proportion of cells inhibited by the treatment, and the Fa-CI plot was generated to evaluate the synergistic effect across different Fa levels. CI<1 indicates synergy, CI=1 indicates additivity and CI>1 indicates antagonism.

EdU proliferation assay. Exponentially growing cells were counted and seeded into 24-well plates at a density of 10,000 cells/well, with three replicate wells for both the control and experimental groups. After 24 h, when cells reached 50-70% confluence, they were subjected to the aforementioned treatments (DMSO, LOP, R or R + LOP). Following 48 h of treatment, the culture medium was discarded, and 200 μl of a 100:1 mixture of medium and EdU solution was added to each well, followed by incubation for 6 h at 37˚C. The mixture was then removed, and the cells were washed three times with PBS, fixed with 4% paraformaldehyde (Biosharp Life Sciences) for 30 min at room temperature and washed once with PBS. Subsequently, 2 mg/ml glycine was added, incubated for 5 min at room temperature and the cells were washed with PBS. The cells were then treated with 0.5% Triton X-100 for 20 min at room temperature and washed three times with PBS. Subsequently, the EdU reaction solution was prepared according to the manufacturer's instructions (kFluor488-EdU Cell Proliferation Detection Kit; cat. no. KGA9608-100; Nanjing KeyGEN Biotech Co., Ltd.), added at 100 μl/well and incubated in the dark for 30 min at room temperature. After three washes with PBS, the cells were stained with DAPI staining solution for 10 min at room temperature, washed three times with PBS and images were captured under an inverted fluorescence microscope.

Colony formation assay. Exponentially growing cells were plated into 6-well plates at a density of 1,000 cells/well. For the irradiation dose-response experiments, cells were exposed to 0, 2, 4, 6, 8 or 10 Gy X-ray irradiation at room temperature (dose rate, 2.0 Gy/min; exposure duration, 1, 2, 3, 4 and 5 min, respectively) to determine the optimal irradiation dose. For the combination experiments, cells were subjected to the aforementioned treatments (DMSO, LOP, R or R + LOP) after small colonies (~30 cells) had formed. The culture medium and drug were replaced every 3 days. After 6-8 days, when colonies (>50 cells) in the control group were clearly visible under microscopy, the medium was discarded. The cells were then washed three times with PBS, fixed with 4% paraformaldehyde for 30 min at room temperature and washed another three times with PBS. Subsequently, the cells were stained with crystal violet for 30 min at room temperature, washed several times with PBS, air-dried and images were captured.

Wound-healing assay. Exponentially growing cells were digested with trypsin to form a single-cell suspension and seeded into 6-well culture plates. The cells were cultured at 37˚C for 24 h until they reached 100% confluence, after which, a vertical scratch was created using a 200-μl pipette tip. After washing three times with PBS to remove detached cells, the cells were cultured in DMEM supplemented with 2% (v/v) FBS. Images were captured under a x4 objective lens to confirm a straight and centered scratch. Subsequently, the cells were subjected to the aforementioned treatments (DMSO, LOP, R or R + LOP). Images were acquired at 24 and 48 h post-treatment, and the wound-healing rate was quantified using ImageJ software (version 1.53t; National Institutes of Health).

Transwell migration assay. Cells were serum-starved for 12 h, harvested and seeded into the upper chambers of 24-well Transwell inserts (pore size, 8 μm; Corning, Inc.) at a density of $2x10^4$ cells/well. The lower chambers were filled with complete medium containing 20% FBS as a chemoattractant. The cells were subjected to the aforementioned treatments (DMSO, LOP, R or R + LOP), and then incubated for 48 h. Non-migrated cells on the upper surface were removed with cotton swabs, whereas cells that had migrated to the lower membrane surface were fixed with 4% paraformaldehyde for 30 min at room temperature, stained with 0.1% crystal violet for 30 min at room temperature and counted under a light microscope in five randomly selected fields per well.

Cell apoptosis detection. Cells were seeded into 6-well plates, subjected to the aforementioned treatments (DMSO, LOP, R or R + LOP), and cultured for 48 h. Cell culture supernatants were then collected. The adherent cells were then digested with EDTA-free trypsin, and the resulting cell suspension was combined with the previously collected supernatants to ensure that both adherent and detached (apoptotic) cells were harvested. The combined suspension was centrifuged at 179 x g for 4 min at room temperature to harvest cell pellets. Following two washes with pre-chilled PBS and centrifugation at 179 x g for 4 min at room temperature, the cells were gently resuspended in pre-chilled 1X Binding Buffer (Annexin V-EGFP Apoptosis Detection Kit; cat. no. C1067S; Beyotime Biotechnology) to adjust the cell density to $1x10^6$ cells/ml, as recommended by the manufacturer. Subsequently, 100 μl cell suspension was incubated with 5 μl Annexin V-EGFP and 5 μl PI for 8-10 min at room temperature in the dark. After the addition of 400 μl pre-chilled 1X Binding Buffer and gentle mixing, flow cytometric analysis was performed within 1 h using a CytoFLEX flow cytometer (Beckman Coulter, Inc.) equipped with CytExpert software (version 2.4.0.28; Beckman Coulter, Inc.). The gating strategy included forward/side scatter gating to exclude debris and doublets, and auto-compensation was performed using single-stained controls. A total of 10,000 events were acquired per sample.

ROS detection. Cells were seeded into 6-well plates at a density of $2x10^5$ cells/well and subjected to the aforementioned treatments (DMSO, LOP, R or R + LOP) and cultured for 48 h. The cells were then trypsinized, centrifuged at 179 x g for 4 min at room temperature and washed three times with pre-chilled PBS. Subsequently, the cells were incubated with DCFH-DA (Reactive Oxygen Species Assay Kit; cat. no. S0033S; Beyotime Biotechnology) and BODIPY-C11 (Lipid Peroxidation Assay Kit; cat. no. S0043S; Beyotime Biotechnology) probes (both diluted 1:1,000 in serum-free DMEM) at 37˚C for 30 min. After three washes with pre-chilled PBS, 500 μl serum-free DMEM was added and flow cytometric analysis was performed within 1 h using a CytoFLEX flow cytometer equipped with CytExpert software (version 2.4.0.28).

Measurement of malondialdehyde (MDA) and GSH. Cells were seeded into 6-well plates at a density of $2x10^5$ cells/well and cultured overnight at 37˚C. The cells were then subjected to the aforementioned treatments and cultured for a total of 48 h (for the R + LOP group, LOP was added 4 h before irradiation and maintained until 48 h after the start of treatment) before analysis. Subsequently, the cells were trypsinized and

centrifuged at 179 x g for 4 min at room temperature. IP lysis buffer (cat. no. P0013; Beyotime Biotechnology) was then added and the cells were lysed on ice for 30 min. After lysis, the supernatant was collected by centrifugation at 12,000 x g for 10 min at 4˚C. The MDA content was determined using a Lipid Peroxidation MDA Assay Kit (cat. no. S0131S; Beyotime Biotechnology) by measuring the absorbance at 532 nm, and the results were expressed as μmol/mg protein. The GSH and GSH disulfide (GSSG) contents were determined using a GSH and GSSG Assay Kit (cat. no. S0053; Beyotime Biotechnology) according to the manufacturers' instructions. Briefly, total GSH was measured by the DTNB-based colorimetric reaction at 412 nm after incubation at 25˚C, and GSSG was measured after GSH was eliminated using the GSH scavenging reagent. The GSH content was calculated as GSH=total GSH-GSSG x 2, and the GSH/GSSG ratio was calculated accordingly. All results were normalized to protein concentration.

Ferroptosis inhibition. Cells were pretreated with 10 μM Ferrostatin-1 (Fer-1; cat. no. HY-100579; MedChemExpress) or 0.1 μM liproxstatin-1 (Lip-1; cat. no. HY-12726; MedChemExpress) for 2 h at 37˚C prior to the aforementioned treatments, and maintained throughout the subsequent 48-h culture period. Erastin (5 μM; cat. no. HY-15763; MedChemExpress) was used alone as a positive control for ferroptosis induction, and cells were treated for 48 h at 37˚C. These pretreatments were applied in the MDA/GSH, Transwell migration and colony formation assays.

Reverse transcription-quantitative PCR (RT-qPCR). Cells were plated into 6-well plates and subjected to the aforementioned treatments (DMSO, LOP, R, or R + LOP) and cultured for a total of 48 h before analysis. For the R + LOP group, LOP was added 4 h before irradiation and maintained until the end of the 48-h period. Total RNA was then extracted using TRIzol® reagent (Invitrogen; Thermo Fisher Scientific, Inc.). Subsequently, 1 μg total RNA was reverse-transcribed into cDNA using a RT kit (HiScript III RT SuperMix for qPCR; cat. no. R323-01; Vazyme Biotech Co., Ltd.) according to the manufacturer's instructions. qPCR was performed using ChamQ Universal SYBR qPCR Master Mix (cat. no. Q711-02; Vazyme Biotech Co., Ltd.) to assess the mRNA expression levels of GPX4 and SLC7A11, and GAPDH was used as an internal reference gene. The thermocycling conditions were as follows: Initial denaturation at 95˚C for 30 sec, followed by 40 cycles at 95˚C for 10 sec, 58˚C for 30 sec and 72˚C for 30 sec, with a final melting curve analysis. The relative mRNA expression levels were determined using the $2^{-\Delta\Delta Cq}$ method (28). The primer sequences were as follows: SLC7A11, forward 5'-TCATTGGAGCAGGAATCTTCA-3', reverse 5'-TTCAGCATAAGACAAAGCTCCA-3'; GPX4, forward 5'-CCCGATACGCTGAGTGTGGTTTG-3', reverse 5'-TGTTCGTTACTCCCTGGCTCCTG-3'; GAPDH, forward 5'-TGTGGGCATCAATGGATTTGG-3' and reverse 5'-ACACCATGTATTCCGGGTCAAT-3'.

Western blot analysis. After treatment, as aforementioned (DMSO, LOP, R or R + LOP), the cells were washed three times with PBS. A lysis buffer mixture was prepared by combining RIPA buffer (cat. no. P0013B; Beyotime Biotechnology,), PMSF and a protease inhibitor cocktail (cat. no. P1005; Beyotime Biotechnology) at a ratio of 100:1:1. Subsequently, 100 μl lysis buffer was added to each well and the plates were incubated on ice for 30 min. Cells were then scraped into 1.5-ml microcentrifuge tubes using a cell scraper. After centrifugation at 11,304 x g for 15 min at 4˚C, the supernatants were collected and the protein concentration was quantified using a BCA protein assay kit. Protein samples were separated by SDS-PAGE on 12% and transferred onto PVDF membranes. The membranes were then incubated overnight at 4˚C with monoclonal antibodies against GPX4 (cat. no. 30388-1-AP; 1:1,000) and SLC7A11 (cat. no. 26864-1-AP; 1:1,000) (both from Proteintech Group, Inc.). After three washes with TBS containing 0.1% (v/v) Tween-20 (10 min each), the membranes were incubated with horseradish peroxidase-conjugated anti-rabbit secondary antibody (cat. no. SA00001-2; 1:5,000; Proteintech Group, Inc.) for 2 h at room temperature. Protein bands were visualized using an ECL detection system (Bio-Rad Laboratories, Inc.). The band intensities were semi-quantified using ImageJ software (version 1.53t) and normalized to the loading control.

Statistical analysis. All experimental data are presented as the mean ± SD from at least three independent experiments. All experiments were performed with at least three independent biological replicates (n=3), each with three technical replicates per condition. Statistical analyses were performed using GraphPad Prism 9 software (Dotmatics). Normality was assessed using the Shapiro-Wilk test and homogeneity of variance was confirmed by Levene's test. Comparisons among multiple groups were performed using one-way ANOVA followed by Tukey's post hoc test. $P<0.05$ was considered to indicate a statistically significant difference.

Results

LOP significantly inhibits the viability of cervical cancer cells. To determine the *in vitro* cytotoxicity of LOP in cervical cancer cells and to assess whether it exerts a synergistic effect with radiotherapy, the inhibitory effect of LOP on the viability of cervical cancer cells was first examined and the optimal X-ray irradiation dose identified. CCK-8 assays revealed that LOP significantly suppressed the viability of SiHa cells, with an IC_{50} of 19.09 μM (Fig. 1A). Increasing concentrations of LOP exerted a marked inhibitory effect on SiHa cell viability in a concentration-dependent manner. Similarly, LOP significantly inhibited the viability of HeLa cells in a concentration-dependent manner, yielding an IC_{50} value of 36.36 μM (Fig. 1B). Colony formation assays were performed to evaluate the inhibitory effect of different doses of X-ray irradiation on SiHa and HeLa cell proliferation (Fig. 1C and D). Colony formation assays revealed a dose-dependent reduction in clonogenic survival following irradiation in both cell lines. At 2-4 Gy, residual colonies remained abundant, indicating insufficient radiation damage to adequately reveal drug-sensitizing effects; at 8-10 Gy, clonogenic survival was nearly abolished, creating a plateau effect that precluded effective discrimination of further inhibition by combination treatment. At 6 Gy, however, both cell lines exhibited notable yet submaximal

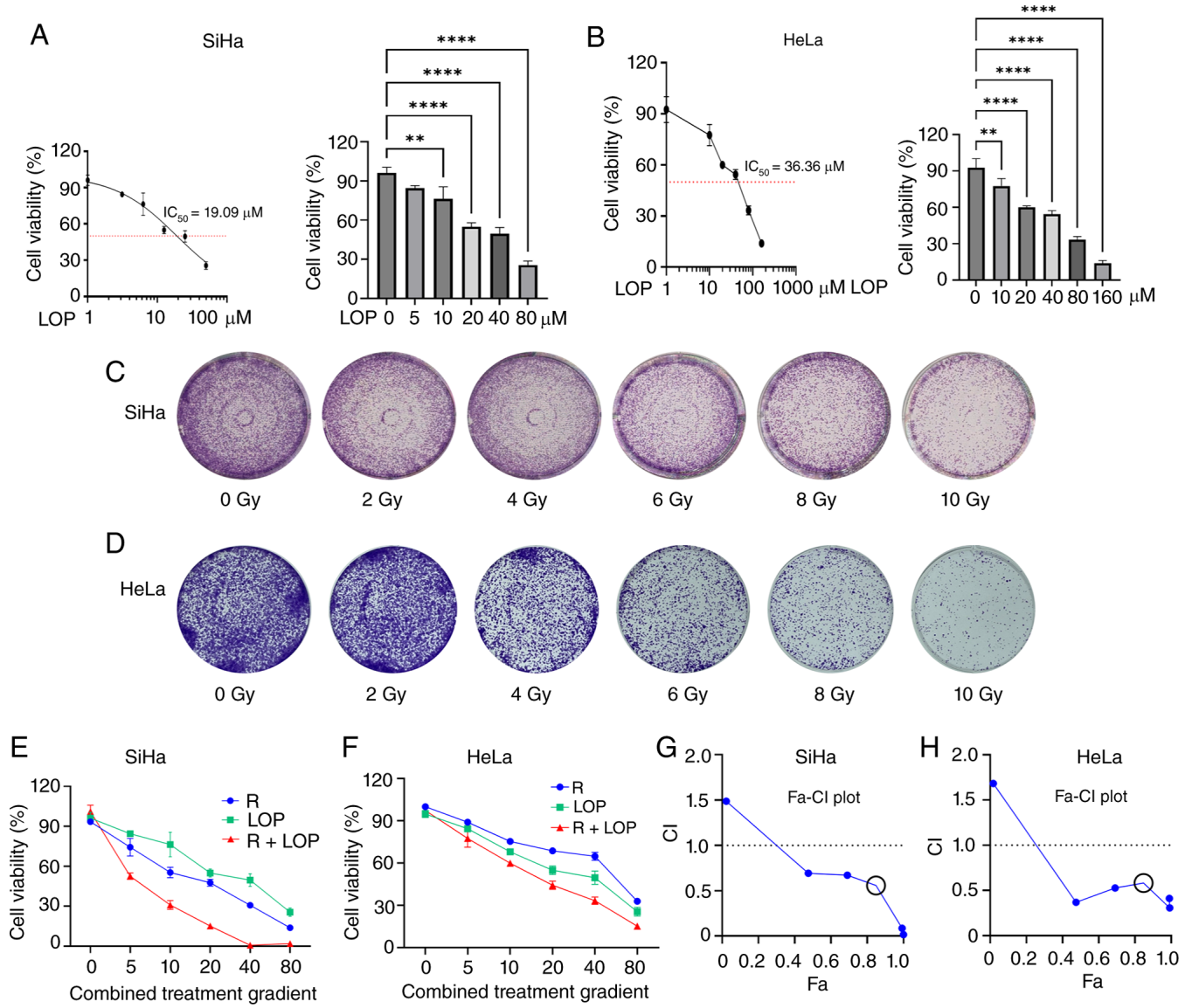

Figure 1. LOP significantly inhibits the proliferation of cervical cancer cells. CCK-8 assay showing the inhibitory effect of LOP on (A) SiHa and (B) HeLa cell proliferation. Colony formation assay evaluating the effect of graded doses of X-ray irradiation on (C) SiHa and (D) HeLa cell clonogenic survival. CCK-8 assay assessing the combinatory effects of LOP and radiotherapy on (E) SiHa and (F) HeLa cells. Cells were treated with graded concentrations of LOP (0-80 μM) in combination with fixed-dose irradiation (0-10 Gy), and cell viability was assessed at 48 h post-treatment. CI analysis using the Chou-Talalay method in (G) SiHa and (H) HeLa cells. The combination of 15 μM LOP and 6 Gy irradiation yielded CI values of 0.58 for SiHa cells and 0.55 for HeLa cells, both of which are <1, indicating a synergistic interaction. All data are presented as the mean ± SD of three independent experiments. Statistical significance was determined using one-way ANOVA. **P<0.01, ****P<0.0001. CCK-8, Cell Counting Kit-8; CI, combination index; Fa, fraction affected; IC_{50}, half-maximal inhibitory concentration; LOP, loperamide; R, radiotherapy.

inhibition (50-60% survival), providing a suitable window for detecting combination effects.

To further evaluate the combined effect, SiHa and HeLa cells were treated with LOP at 0, 5, 10, 20, 40 and 80 μM, each paired with a fixed irradiation dose of 0, 2, 4, 6, 8 and 10 Gy, respectively (0 μM + 0 Gy, 5 μM + 2 Gy, 10 μM + 4 Gy, 20 μM + 6 Gy, 40 μM + 8 Gy and 80 μM + 10 Gy). Cell viability was assessed using a CCK-8 assay at 48 h post-treatment (Fig. 1E and F). CI analysis was performed using the Chou-Talalay method, and the Fa values were calculated for each single agent and their combination. Fa-CI analysis demonstrated that the combination of LOP and irradiation was synergistic (CI <1) across the evaluated Fa range (Fig. 1G and H). Among the tested combinations, 20 μM LOP combined with 6 Gy irradiation showed the strongest synergy; however, this concentration exceeded the IC_{50} of SiHa cells (19.09 μM). Therefore, 15 μM LOP, a sub-IC_{50} concentration that retained synergy, was selected. At this concentration, the combination with 6 Gy irradiation yielded CI values of 0.58 for SiHa cells and 0.55 for HeLa cells, both <1, confirming a synergistic interaction (Fig. 1G and H). Based on these results, 15 μM LOP and 6 Gy irradiation were selected for subsequent combination experiments in both cell lines.

LOP enhances the inhibitory effect of radiotherapy on cervical cancer cell proliferation. To investigate whether LOP can enhance the radiosensitivity of cervical cancer cells, two cervical cancer cell lines (SiHa and HeLa) were treated with LOP alone or in combination with irradiation.

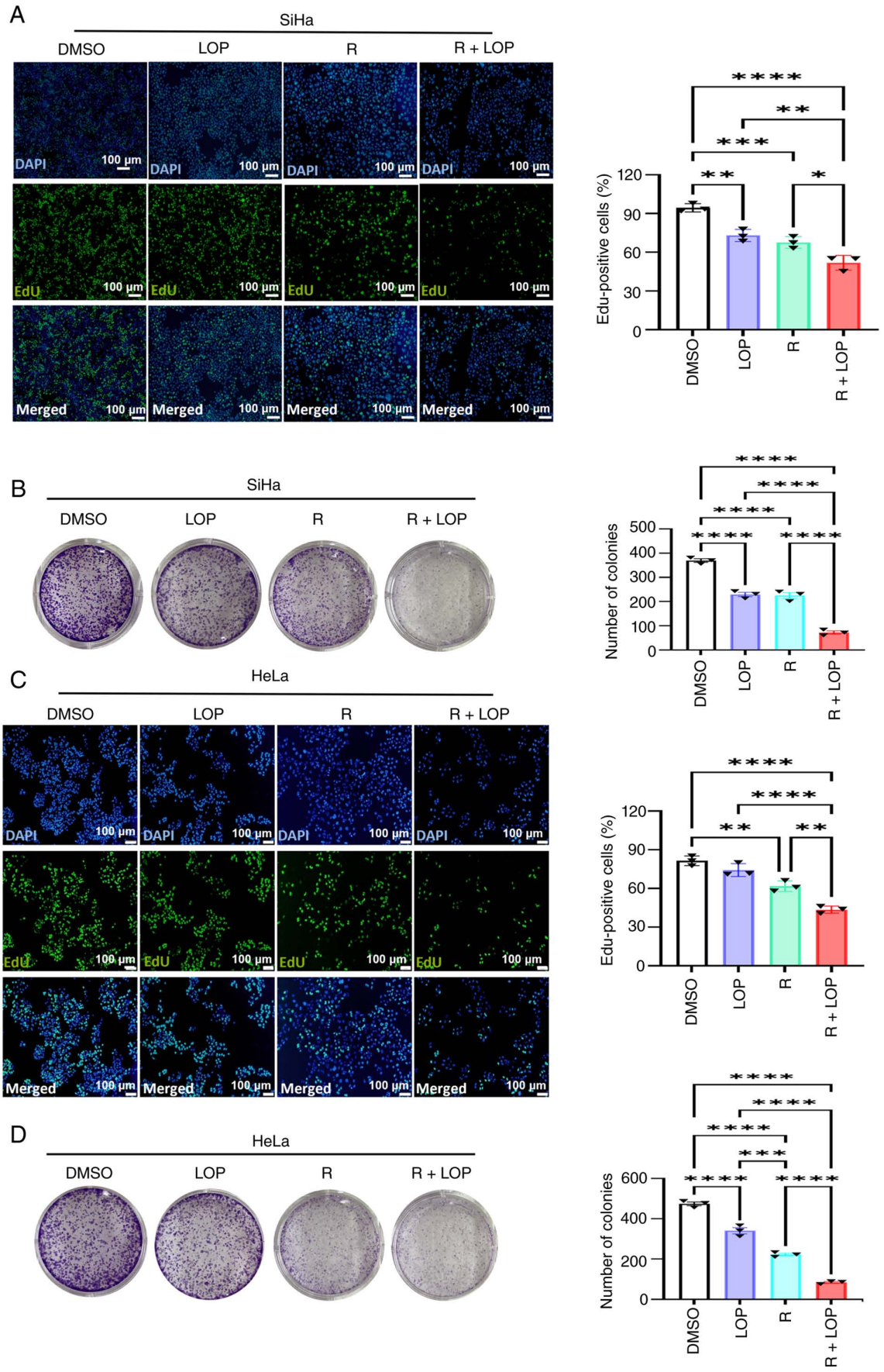

Figure 2. LOP enhances the inhibitory effect of radiotherapy on cervical cancer cell proliferation. (A) EdU assay detecting the proliferation of SiHa cells treated with LOP combined with radiotherapy. (B) Colony formation assay assessing the clonogenic survival of SiHa cells treated with LOP combined with radiotherapy. (C) EdU assay detecting the proliferation of HeLa cells treated with LOP combined with radiotherapy. (D) Colony formation assay assessing the clonogenic survival of HeLa cells treated with LOP combined with radiotherapy. All data are presented as the mean ± SD of three independent experiments. Statistical significance was determined using one-way ANOVA. *P<0.05, **P<0.01, ***P<0.001, ****P<0.0001. LOP, loperamide; R, radiotherapy.

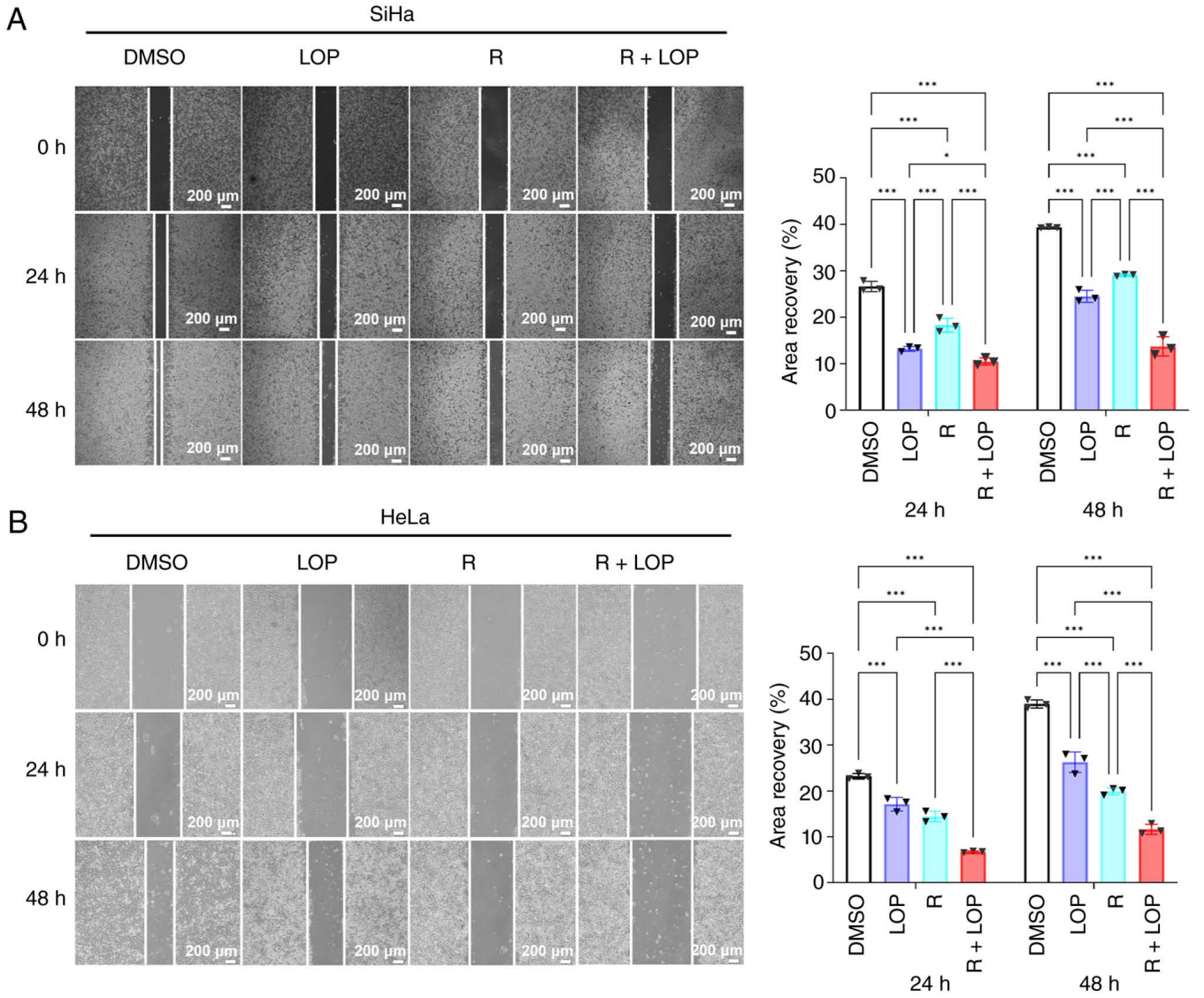

Figure 3. LOP enhances the inhibitory effect of radiotherapy on cervical cancer cell migration. Wound-healing assay and quantification of migration in (A) SiHa and (B) HeLa cells treated with LOP combined with radiotherapy. Apoptosis was detected using an Annexin V-EGFP Apoptosis Detection Kit; Annexin V-EGFP (green fluorescence) was detected in the FITC channel and PI (red fluorescence) in the PE channel. All data are presented as the mean ± SD of three independent experiments. Statistical significance was determined using one-way ANOVA. *P<0.05; ***P<0.001. LOP, loperamide; R, radiotherapy.

The inhibitory efficiency on cell proliferation was assessed using an EdU assay. The results demonstrated that both LOP alone and LOP combined with radiotherapy significantly suppressed the proliferation of SiHa cells, and the inhibitory effect was markedly enhanced in the combination treatment group (Fig. 2A). Colony formation assays revealed that LOP significantly reduced the number of colonies formed by SiHa cells, and the inhibitory effect was further strengthened upon combined treatment with radiotherapy (Fig. 2B). Similarly, LOP combined with radiotherapy significantly inhibited the proliferation and colony formation ability of HeLa cells (Fig. 2C and D).

LOP enhances the inhibitory effect of radiotherapy on cervical cancer cell migration. Tumor cell migration is a key factor in tumor invasion and metastasis (29). Accordingly, wound-healing assays were performed to determine whether LOP could enhance the inhibitory effect of radiotherapy on the migration of cervical cancer cells. The results demonstrated that, compared with in the control group, the wound closure rates of both cell lines in the LOP group, radiotherapy alone group and LOP plus radiotherapy group were significantly decreased at 24 and 48 h. Moreover, compared with in the radiotherapy alone group, cell migration was markedly arrested and almost abolished in the combination treatment group (Fig. 3A and B). Collectively, these findings indicated that LOP combined with radiotherapy may significantly suppress the migratory capacity of cervical cancer cells.

LOP enhances radiotherapy-induced apoptosis in cervical cancer cells. The balance between proliferation and apoptosis determines the sensitivity of tumor cells to therapy. The current study subsequently assessed whether LOP affects radiotherapy-induced apoptosis using Annexin V-PI double staining. Flow cytometric analysis in two cervical cancer cell

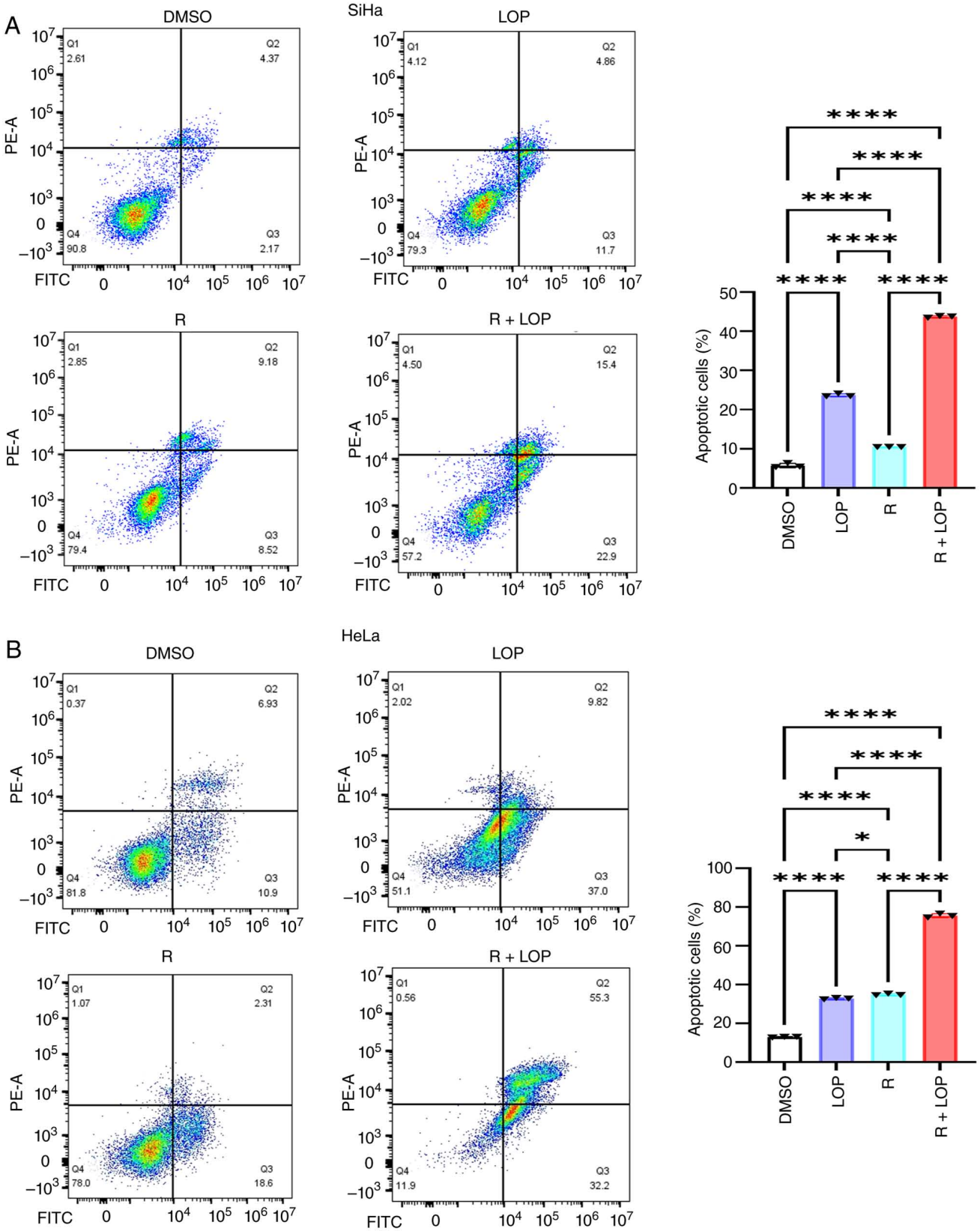

Figure 4. LOP enhances radiotherapy-induced apoptosis in cervical cancer cells. Flow cytometric analysis and quantification of apoptosis in (A) SiHa and (B) HeLa cells treated with LOP combined with radiotherapy. All data are presented as the mean ± SD of three independent experiments. Statistical significance was determined using one-way ANOVA. *P<0.05, ****P<0.0001. LOP, loperamide; R, radiotherapy.

lines (SiHa and HeLa) demonstrated that, compared with in the control group, the radiotherapy alone group, LOP alone group and LOP plus radiotherapy group all significantly increased the proportion of late apoptotic cells. Moreover, the combination of LOP and radiotherapy induced a markedly greater apoptotic effect than radiotherapy alone (Fig. 4A and B).

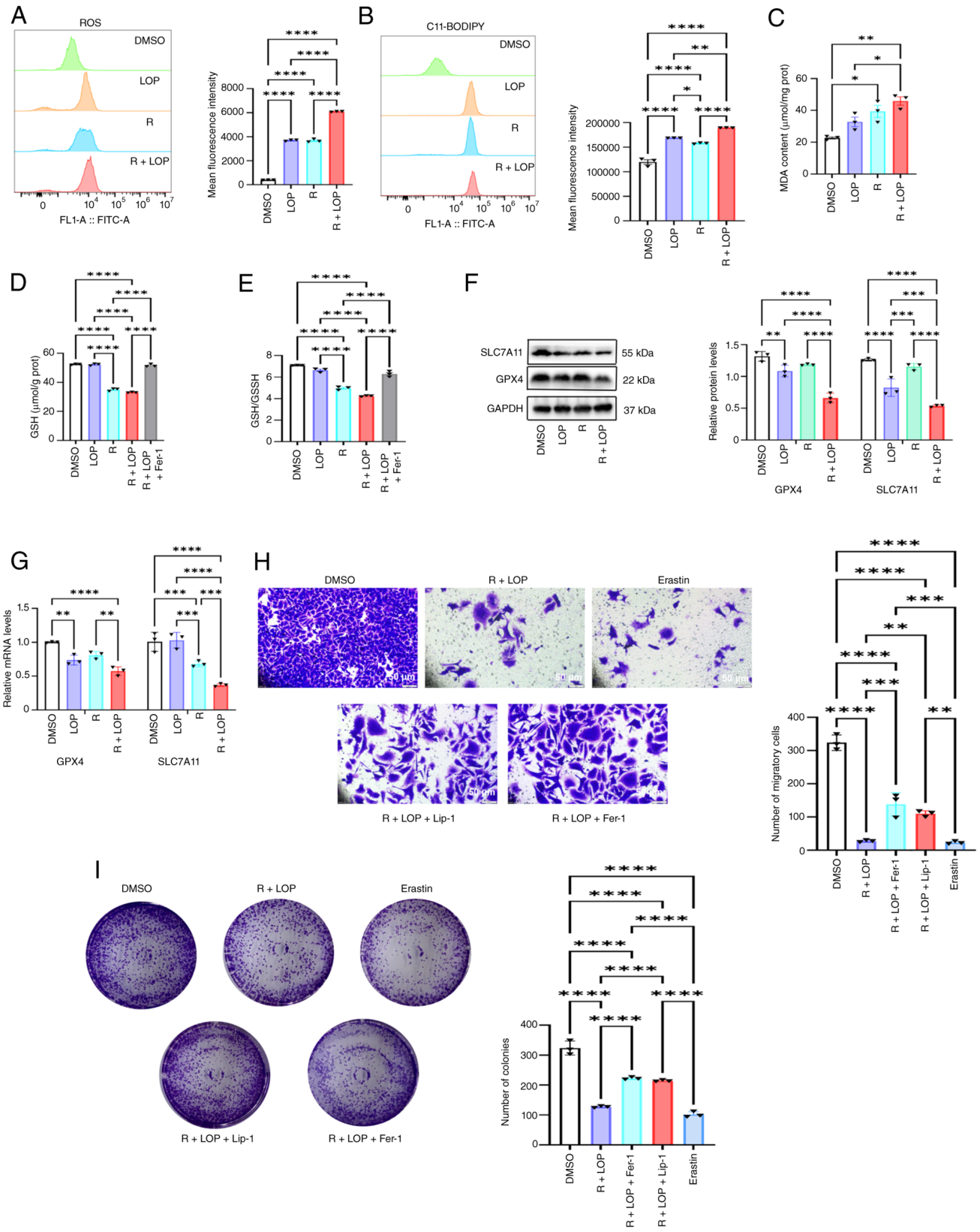

Figure 5. LOP promotes radiotherapy-induced ferroptosis in cervical cancer cells. Flow cytometric analysis and quantification of (A) intracellular ROS levels (DCFH-DA) and (B) lipid peroxidation (BODIPY-C11) in HeLa cells treated with LOP combined with radiotherapy. (C) MDA levels, (D) GSH levels and (E) GSH/GSSG ratio in HeLa cells under the indicated treatments. (F) Protein expression and semi-quantification of SLC7A11 and GPX4 in HeLa cells treated with LOP combined with radiotherapy detected using western blotting. (G) mRNA expression levels of SLC7A11 and GPX4 in HeLa cells analyzed using quantitative PCR. (H) Transwell migration assay. HeLa cells were treated with DMSO vehicle control, R + LOP, R + LOP + Fer-1 (10 μM), R + LOP + Lip-1 (0.1 μM) or Erastin (5 μM) alone as a positive control. Representative images of crystal violet-stained migrated cells (scale bar, 50 μm) and quantification of migratory cells are shown. (I) Colony formation assay. Representative images of crystal violet-stained colonies and quantification of colony numbers are shown. All data are presented as the mean ± SD of three independent experiments. Statistical significance was determined using one-way ANOVA. *P<0.05, **P<0.01, ***P<0.001, ****P<0.0001. Fer-1, Ferrostatin-1; GPX4, GSH peroxidase 4; GSH, glutathione; GSSG, GSH disulfide; Lip-1, liproxstatin-1; LOP, loperamide; MDA, malondialdehyde; R, radiotherapy; ROS, reactive oxygen species; SLC7A11, solute carrier family 7 member 11.

LOP promotes radiotherapy-induced ferroptosis in cervical cancer cells. To explore the molecular mechanism underlying LOP-enhanced radiosensitivity in cervical cancer cells, intracellular ROS (detected using DCFH-DA) and lipid peroxidation (detected using BODIPY-C11) in HeLa cells were determined using flow cytometry. Compared with in the control group, ROS and BODIPY-C11 levels in HeLa cells were significantly elevated in the radiotherapy alone, LOP alone and combination groups, with a more marked increase observed in the combination group relative to radiotherapy alone (Fig. 5A and B). These findings indicated that LOP combined with radiotherapy may significantly promote lipid peroxidation and induce oxidative stress. In addition, MDA and GSH levels, as well as the GSH/GSSG ratio, were measured in HeLa cells. The combination treatment resulted in the highest MDA levels, and the lowest GSH levels and GSH/GSSG ratio among all groups (Fig. 5C-E).

Notably, the ferroptosis inhibitor Fer-1 partially reversed these effects induced by LOP plus radiotherapy, suggesting that ferroptosis contributes to the observed biochemical changes (Fig. 5D and E). To validate this hypothesis, RT-qPCR and western blot analysis were performed in HeLa cells. Western blot analysis demonstrated that SLC7A11 and GPX4 protein levels were decreased in all treatment groups, and the reduction was more significant in the combination group relative to radiotherapy alone (Fig. 5F). Consistently, qPCR revealed that the mRNA expression levels of SLC7A11 and GPX4 were downregulated in the treatment groups compared with in the control group, with a more pronounced reduction in the combination group than in the radiotherapy alone group (Fig. 5G). To further explore the involvement of ferroptosis in the anti-migratory effect of LOP and radiation, Transwell migration assays were performed following treatment with Fer-1 (10 μM) and Lip-1 (0.1 μM); the results demonstrated that both ferroptosis inhibitors partially reversed the inhibition of cell migration induced by the combination treatment, whereas Erastin (5 μM), a ferroptosis inducer tested alone as a positive control, inhibited cell migration to a similar extent as the combination treatment (Fig. 5H). Colony formation assays further confirmed that Fer-1 and Lip-1 partially reversed the combination-induced suppression of clonogenic survival, whereas erastin, tested alone as a positive control, reduced colony formation to a similar extent as the combination treatment (Fig. 5I). These data support the involvement of ferroptosis in the observed effects, although they do not exclude contributions from other cell death pathways. Core ferroptosis experiments (ROS, BODIPY-C11, RT-qPCR and western blotting for GPX4/SLC7A11, and Fer-1 rescue) were also performed in SiHa cells, yielding results consistent with those obtained in HeLa cells (Fig. S1).

Discussion

Cervical cancer is one of the most prevalent malignant tumors in women worldwide in terms of both incidence and mortality, and radiotherapy represents one of its standard therapeutic modalities. However, radioresistance of tumor cells remains a major cause of treatment failure and recurrence. Therefore, exploring effective adjuvant strategies to radiosensitize tumors is clinically important (30). Notably, ferroptosis, an iron-dependent form of regulated cell death characterized by the accumulation of lipid peroxides, has attracted extensive attention in cancer therapy (31). Emerging evidence has suggested a potential link between ferroptosis and radiosensitivity, providing a novel strategy to enhance radiotherapy efficacy (32-34). The present study aimed to investigate whether the clinically used drug LOP could act as a radiosensitizer and enhance the radiosensitivity of cervical cancer cells by regulating the ferroptosis pathway.

The IC_{50} values of LOP in cervical cancer cell lines (19.09 μM for SiHa and 36.36 μM for HeLa) provided the basis for subsequent combination experiments. The combined treatment of LOP and radiotherapy exerted synergistic inhibitory effects on cell proliferation and migration, as confirmed by CI analysis (CI<1 for both cell lines). This synergy may arise from the convergence of radiotherapy-induced DNA damage and LOP-triggered ferroptotic pathways, thereby amplifying the final cytotoxic effect. A complex causal relationship exists between the elevated ROS levels and increased apoptosis induced by the combined treatment. Radiotherapy alone generates ROS via ionizing radiation, which directly damages DNA and induces mitochondrial apoptosis. The addition of LOP may further exacerbate intracellular oxidative stress. Notably, the markedly increased lipid peroxidation detected specifically by the C11 BODIPY probe suggested that cell death was not solely mediated by the canonical apoptotic pathway. In fact, the core feature of ferroptosis is the aberrant accumulation of lipid peroxides, which is mechanistically and morphologically distinct from apoptosis.

Both apoptosis and ferroptosis were indicated to be induced by the combined treatment of LOP and irradiation. Ferroptotic markers, including ROS accumulation, lipid peroxidation, MDA elevation and GSH depletion, exhibited pronounced changes following combination treatment, and the ferroptosis inhibitor Fer-1 partially reversed these biochemical effects. Additionally, LOP treatment was associated with downregulation of the SLC7A11/GPX4 axis, which constitutes a core defense mechanism against ferroptosis. GSH serves as an essential reducing substrate for GPX4, which reduces lipid hydroperoxides to non-toxic alcohols and thus constitutes a core barrier against ferroptosis. SLC7A11 mediates the uptake of extracellular cystine for GSH synthesis, and its inhibition directly limits GSH production (35,36). Therefore, the downregulation of both SLC7A11 and GPX4 by LOP combined with radiotherapy likely disrupts this antioxidant defense system, favoring ferroptotic cell death. However, it is important to note that the functional rescue experiments with ferroptosis inhibitors demonstrated only partial reversal of the combination-induced effects on cell migration and clonogenic survival. Furthermore, apoptosis was also significantly induced by the combination treatment. Given that apoptosis evasion is a well-recognized mechanism of radioresistance, the concurrent induction of both apoptotic and ferroptotic pathways may collectively contribute to the enhanced radiosensitivity observed in the current study. At present, the available data do not permit a definitive conclusion regarding the relative dominance of ferroptosis versus apoptosis. It is therefore hypothesized that while ferroptosis represents a newly identified and mechanistically relevant pathway, the radiosensitizing effect of LOP is likely mediated by the

convergent actions of multiple cell death mechanisms. The functional interplay between these pathways and their relative contributions warrant further investigation using systematic pharmacological and genetic approaches.

Notably, the present findings are consistent with the results of previous reports demonstrating that ferroptosis inducers or modulators, such as propofol and curcumin, enhance the sensitivity of various cancer types, including cervical cancer, hepatocellular carcinoma and breast cancer to anticancer therapies through the SLC7A11/GPX4 axis (37-40). To the best of our knowledge, the present study is the first to explicitly link the clinically used drug LOP to radiosensitization in cervical cancer via ferroptosis mediated by the SLC7A11/GPX4 axis.

However, several limitations are acknowledged in the present study. First, the micromolar concentrations of LOP used in the *in vitro* studies are substantially higher than the plasma concentrations typically achieved with standard oral antidiarrheal dosing, primarily due to extensive first-pass metabolism and P-glycoprotein-mediated efflux. Additionally, the well-documented cardiac toxicity of LOP, particularly QT interval prolongation, further limits the feasibility of dose escalation (41). Potential strategies to overcome these limitations include local or regional delivery approaches (such as intratumoral injection or nanoparticle-based formulations) to achieve higher local concentrations while minimizing systemic exposure, or the development of more potent ferroptosis-inducing analogs with improved pharmacokinetic profiles. Second, the present findings were obtained in conventional parental SiHa and HeLa cell lines, which are not intrinsically radioresistant. While significant synergy was observed in these models, the translational relevance of these findings to clinically radioresistant settings remain to be established. Future studies using established radioresistant sublines or patient-derived radioresistant models are warranted to evaluate the efficacy of LOP in clinically refractory settings. Third, the present study did not include a non-malignant cervical epithelial cell line to evaluate the cancer selectivity of LOP; future studies are warranted to assess its safety profile in normal tissues. Additionally, future *in vivo* studies are required to validate the efficacy and safety of this combination strategy, and to explore the expression levels of GPX4 or SLC7A11 as potential biomarkers for predicting response to LOP-radiotherapy combination, thereby enabling precise patient stratification.

In conclusion, the present findings demonstrated that LOP enhances the radiosensitivity of cervical cancer cells, with ferroptosis induction via inhibition of the SLC7A11/GPX4 axis as a contributing mechanism. Both apoptosis and ferroptosis were induced by the combined treatment, suggesting convergent contributions from multiple cell death pathways. These observations provide a rationale for further investigation into LOP as a potential radiosensitizing agent.

Acknowledgements

The authors would like to thank Professor Te Zhang (Biomedical Research Institute of Hubei University of Medicine) for his technical assistance with flow cytometry.

Funding

This work was supported by the Scientific and Technological Project of Shiyan City of Hubei Province (grant no. 25Y009), the Open Project of Hubei Regional Medical Center for Geriatric Disease (Sinopharm Dongfeng General Hospital, Hubei University of Medicine) (grant no. GDMC2026003), the Innovative Research Program for Graduates of Hubei University of Medicine (grant no. YC2026020) and the Training Program of Innovation and Entrepreneurship for Undergraduates (grant no. S202610929030).

Availability of data and materials

The data generated in the present study may be requested from the corresponding author.

Authors' contributions

JK and FYW designed the experiments. HRG and HXL performed the experiments and analyzed the data. SKT and YKZ performed the flow cytometry experiments. FYW and JK confirm the authenticity of all the raw data. JK wrote the manuscript. All authors read and approved the final manuscript.

Ethics approval and consent to participate

Not applicable.

Patient consent for publication

Not applicable.

Competing interests

The authors declare that they have no competing interests.

References

1. Wu J, Jin Q, Zhang Y, Ji Y, Li J, Liu X, Duan H, Feng Z, Liu Y, Zhang Y, *et al*: Global burden of cervical cancer: Current estimates, temporal trend and future projections based on the GLOBOCAN 2022. J Natl Cancer Cent 5: 322-329, 2025.
2. Bray F, Laversanne M, Sung H, Ferlay J, Siegel RL, Soerjomataram I and Jemal A: Global cancer statistics 2022: GLOBOCAN estimates of incidence and mortality worldwide for 36 cancers in 185 countries. CA Cancer J Clin 74: 229-263, 2024.
3. Singh D, Vignat J, Lorenzoni V, Eslahi M, Ginsburg O, Lauby-Secretan B, Arbyn M, Basu P, Bray F and Vaccarella S: Global estimates of incidence and mortality of cervical cancer in 2020: a baseline analysis of the WHO Global Cervical Cancer Elimination Initiative. Lancet Glob Health 11: e197-e206, 2023.
4. Neibart SS, Lin LL, Einstein MH, Teoh D, Leath CA and Chino J: Minimum standards for radiation therapy in the treatment of cervical cancer in the U.S.: A consensus statement by SGO, ASTRO, and ABS addressing the WHO Cervical Cancer Elimination Campaign goals. Gynecol Oncol 200: 180-185, 2025.
5. Wu Y, Song Y, Wang R and Wang T: Molecular mechanisms of tumor resistance to radiotherapy. Mol Cancer 22: 96, 2023.
6. Wegge M, Dok R, Dubois LJ and Nuyts S: Hypoxia induces a mitotic survival advantage after radiotherapy in head and neck cancer cells. Int J Cancer 159: 1042-1055, 2026.
7. Sia J, Szmyd R, Hau E and Gee HE: Molecular mechanisms of Radiation-induced cancer cell death: A primer. Front Cell Dev Biol 8: 41, 2020.

8. Liu S, Wang W, Hu S, Jia B, Tuo B, Sun H, Wang Q, Liu Y and Sun Z: Radiotherapy remodels the tumor microenvironment for enhancing immunotherapeutic sensitivity. Cell Death Dis 14: 679, 2023.
9. Begg AC, Stewart FA and Vens C: Strategies to improve radiotherapy with targeted drugs. Nat Rev Cancer 11: 239-253, 2011.
10. Kim BM, Hong Y, Lee S, Liu P, Lim JH, Lee YH, Lee TH, Chang KT and Hong Y: Therapeutic implications for overcoming radiation resistance in cancer therapy. Int J Mol Sci 16: 26880-26913, 2015.
11. Chen F, Kang R, Tang D and Liu J: Ferroptosis: Principles and significance in health and disease. J Hematol Oncol 17: 41, 2024.
12. Jiang X, Stockwell BR and Conrad M: Ferroptosis: Mechanisms, biology and role in disease. Nat Rev Mol Cell Biol 22: 266-282, 2021.
13. Lee J and Roh JL: Inducing ferroptosis to enhance radiotherapy in head and neck cancer: Mechanisms, radiosensitization strategies, and normal tissue considerations. Cells 15: 812, 2026.
14. Xiao H, Jiang N, Zhang H, Wang S, Pi Q, Chen H, He X, Luo W, Lu Y, Deng Y and Zhong Z: Inhibitors of APE1 redox and ATM synergistically sensitize osteosarcoma cells to ionizing radiation by inducing ferroptosis. Int Immunopharmacol 139: 112672, 2024.
15. Wu M, Pu C, Weng W, Yin F, Zhang L, Xu C, Li M, Cao C and Hu W: Fuzuloparib enhances radiosensitivity of gain-of-function mutant p53 R273H NSCLC by promoting SLC7A11/GSH/GPX4 axis mediated ferroptosis. NPJ Precis Oncol 10: 336, 2026.
16. Wang X, Shi W, Li M, Xin Y and Jiang X: RSL3 sensitizes glioma cells to ionizing radiation by suppressing TGM2-dependent DNA damage repair and epithelial-mesenchymal transition. Redox Biol 78: 103438, 2024.
17. Kerkhove L, Geirnaert F, Rifi AL, Law KL, Gutiérrez A, Oudaert I, Corbet C, Gevaert T, Dufait I and De Ridder M: Repurposing sulfasalazine as a radiosensitizer in hypoxic human colorectal cancer. Cancers (Basel) 15: 2363, 2023.
18. Wu Y, Chen D, Wang X, Song M, Wu J, Wu S and Liao K: Dihydroartemisinin targets GPX4 to induce autophagy-dependent ferroptosis and reduce radioresistance in triple-negative breast cancer. Free Radic Biol Med 246: 35-50, 2026.
19. Pan X, Lin Z, Jiang D, Yu Y, Yang D, Zhou H, Zhan D, Liu S, Peng G, Chen Z and Yu Z: Erastin decreases radioresistance of NSCLC cells partially by inducing GPX4-mediated ferroptosis. Oncol Lett 17: 3001-3008, 2019.
20. Zhao L, Zhou X, Xie F, Zhang L, Yan H, Huang J, Zhang C, Zhou F, Chen J and Zhang L: Ferroptosis in cancer and cancer immunotherapy. Cancer Commun (Lond) 42: 88-116, 2022.
21. Ishikawa K, Matsuoka Y, Shinohara K, Inoue J, Yano H, Eto T, Yamamoto T, Yamana K, Gohara S, Takeshita H, *et al*: Involvement of ferroptosis-defensive xCT/GPX4 axis in radioresistance and its impacts on prognosis in oral squamous cell carcinoma. Oral Sci Int 21: 359-372, 2024.
22. Wu PE and Juurlink DN: Loperamide cardiac toxicity: Pathophysiology, presentation, and management. Can J Cardiol 38: 1378-1383, 2022.
23. Wu PE and Juurlink DN: Clinical review: Loperamide toxicity. Ann Emerg Med 70: 245-252, 2017.
24. Elia SG, Al-Karmalawy AA, Nasr MY and Elshal MF: Loperamide potentiates doxorubicin sensitivity in triple-negative breast cancer cells by targeting MDR1 and JNK and suppressing mTOR and Bcl-2: In vitro and molecular docking study. J Biochem Mol Toxicol 36: e22938, 2022.
25. Meyer N, Henkel L, Linder B, Zielke S, Tascher G, Trautmann S, Geisslinger G, Münch C, Fulda S, Tegeder I and Kögel D: Autophagy activation, lipotoxicity and lysosomal membrane permeabilization synergize to promote pimozide- and loperamide-induced glioma cell death. Autophagy 17: 3424-3443, 2021.
26. Wandel C, Kim R, Wood M and Wood A: Interaction of morphine, fentanyl, sufentanil, alfentanil, and loperamide with the efflux drug transporter P-glycoprotein. Anesthesiology 96: 913-920, 2002.
27. Chou TC: Drug combination studies and their synergy quantification using the Chou-Talalay method. Cancer Res 70: 440-446, 2010.
28. Livak KJ and Schmittgen TD: Analysis of relative gene expression data using real-time quantitative PCR and the 2(-Delta Delta C(T)) method. Methods 25: 402-408, 2001.
29. Bravo-Cordero JJ, Hodgson L and Condeelis J: Directed cell invasion and migration during metastasis. Curr Opin Cell Biol 24: 277-283, 2012.
30. Kuwahara Y, Tomita K, Habibi Roudkenar M, Mohammadi Roushandeh A, Sato T and Kurimasa A: The reversibility of cancer radioresistance: A novel potential way to identify factors contributing to tumor radioresistance. Hum Cell 36: 963-971, 2023.
31. Dixon SJ, Lemberg KM, Lamprecht MR, Skouta R, Zaitsev EM, Gleason CE, Patel DN, Bauer AJ, Cantley AM, Yang WS, *et al*: Ferroptosis: An iron-dependent form of nonapoptotic cell death. Cell 149: 1060-1072, 2012.
32. An S, Han A, Lin Z and Quan H: Targeting ferroptosis in cervical cancer: Mechanistic insights and therapeutic opportunities. Cell Signal 136: 112122, 2025.
33. Li L, Bo Y, Xue D and Qin L: Ferroptosis-immune crosstalk in cervical cancer: Mechanisms and therapeutic implications. Front Immunol 16: 1657905, 2025.
34. Lei G, Zhang Y, Koppula P, Liu X, Zhang J, Lin SH, Ajani JA, Xiao Q, Liao Z, Wang H and Gan B: The role of ferroptosis in ionizing radiation-induced cell death and tumor suppression. Cell Res 30: 146-162, 2020.
35. Zhang W, Liu Y, Liao Y, Zhu C and Zou Z: GPX4, ferroptosis, and diseases. Biomed Pharmacother 174: 116512, 2024.
36. Wang F, Wang L and Bai Y: Research progress of ferroptosis in cervical cancer treatment. Ann Med 58: 2611208, 2026.
37. Zhao MY, Liu P, Sun C, Pei LJ and Huang YG: Propofol augments Paclitaxel-induced cervical cancer cell ferroptosis in vitro. Front Pharmacol 13: 816432, 2022.
38. Lang X, Green MD, Wang W, Yu J, Choi JE, Jiang L, Liao P, Zhou J, Zhang Q, Dow A, *et al*: Radiotherapy and immunotherapy promote tumoral lipid oxidation and ferroptosis via synergistic repression of SLC7A11. Cancer Discov 9: 1673-1685, 2019.
39. Wu PH, Chang WM, Chiou JF, Kuo CC, Wang WJ and Lee HL: Overcoming radioresistance in hepatocellular carcinoma through ferroptosis modulation and exosomal biomarkers. Int J Radiation Oncol Biol Physics 123: e520, 2025.
40. Li R, Zhang J, Zhou Y, Gao Q, Wang R, Fu Y, Zheng L and Yu H: Transcriptome investigation and in vitro verification of Curcumin-induced HO-1 as a feature of ferroptosis in breast cancer cells. Oxid Med Cell Longev 2020: 3469840, 2020.
41. Lammoglia BC, Hasselmann G, Pires-Oliveira M, Duarte Nicolau LA, Rolim Medeiros JV, Sabia Tallo F, Omar Taha M, Yamaguti Lima R, Caricati-Neto A and Menezes-Rodrigues FS: Risk of cardiac lesion with chronic and acute use of Loperamide-an integrative review. J Cardiovasc Dev Dis 9: 431, 2022.

Copyright © 2026 Guo et al. This work is licensed under a Creative Commons Attribution-NonCommercial-NoDerivatives 4.0 International (CC BY-NC-ND 4.0) License.